



## Promoting effect of cerium on MoVTeNb mixed oxide catalyst for oxidative dehydrogenation of ethane to ethylene

Yang Sik Yun<sup>a,1</sup>, Minzae Lee<sup>a,1</sup>, Jongbaek Sung<sup>a</sup>, Danim Yun<sup>a</sup>, Tae Yong Kim<sup>a</sup>, Hongseok Park<sup>a</sup>, Kyung Rok Lee<sup>a</sup>, Chyan Kyung Song<sup>a</sup>, Younhwa Kim<sup>a</sup>, Joongwon Lee<sup>b</sup>, Young-Jong Seo<sup>b</sup>, In Kyu Song<sup>c</sup>, Jongheop Yi<sup>a,\*</sup>

<sup>a</sup> World Class University Program of Chemical Convergence for Energy & Environment, Institute of Chemical Processes, School of Chemical and Biological Engineering, Seoul National University, Seoul 151-742, Republic of Korea

<sup>b</sup> Lotte Chemical Corporation, Gajeongbuk-ro, Yuseong-gu, Daejeon 305-726, Republic of Korea

<sup>c</sup> School of Chemical and Biological Engineering, Institute of Chemical Processes, Seoul National University, Shinlim-dong, Kwanak-gu, Seoul 151-744, Republic of Korea



### ARTICLE INFO

#### Keywords:

Oxidative dehydrogenation  
Ethane  
Ethylene  
Ce  
MoVTeNbO

### ABSTRACT

Ce-incorporated MoVTeNbO catalysts were developed to enhance ethylene productivity of oxidative dehydrogenation of ethane (ODHE) to ethylene. Structural characterizations (XRD, TEM, STEM, Raman, and UV-vis DRS) and DFT calculations revealed that Ce atoms were incorporated into MoVTeNbO framework with maintaining its unique structure (*M1* phase), which is active phase for ODHE. The reducibility of the catalysts was enhanced and both  $V^{5+}$  and the lattice oxygen species available to ODHE reaction were enriched by incorporation of Ce, confirmed by TPR, XPS, and pulse injection method, respectively. These improved properties enhanced the conversion of ethane while maintaining their excellent selectivity to ethylene for MoVTeNbCeO catalysts. It is noteworthy that 56.2% of ethane conversion and 95.4% of ethylene selectivity were retained for 200 h over MoVTeNbCeO-0.1 catalyst. Ethylene productivity was calculated to be  $1.11 \text{ kgC}_2\text{H}_4/\text{kg}_{\text{cat}} \text{ h}$ . The developed catalyst exhibits substantial level of ethylene productivity and stability having the possibility with low production of  $\text{CO}_x$  to make a step forward for industrialization of oxidative dehydrogenation of ethane.

### 1. Introduction

Ethylene is a primary building block for the production of value-added chemicals such as polyethylene, ethylene oxide, and, styrene [1–3]. Most of ethylene has been produced by steam cracking of ethane and thermal cracking of petrochemicals (e.g. naphtha) in commercial process. However, the processes are operated at high temperature ( $> 800^\circ\text{C}$ ), resulting in high energy consumption and undesired side reactions [1]. In addition, the processes suffer from coke depositions and environmentally harmful gases ( $\text{CO}_2$  and  $\text{NO}_x$ ) emissions [2]. Especially, large production of greenhouse gas ( $\text{CO}_2$ , 1.5–3 times per ethylene production) is considered as one of major drawbacks in conventional processes [3]. The increasing demand for minimizing the negative environmental impact and the necessity of efficient process promote a development of alternative reaction process for the production of ethylene.

The oxidative dehydrogenation of ethane (ODHE) has attracted considerable attention as an efficient process due to its low energy costs, low

deactivation, availability of the reactant from shale gas instead of petrochemical feedstock, and low greenhouse-gas emission [4–6]. A variety of metal oxide catalysts have been studied for the ODHE reaction, as exemplified by Ni-based [1,7–11], Mo-V-based [12–15], and La–b ased mixed oxides [16], supported alkali chlorides [17–19], and supported noble metals [20,21], etc. Among them, MoVTeNbO catalyst is one of the most promising catalysts for ODHE as well as propane selective oxidation [22,23]. In previous researches, it shows high ethane conversion and ethylene selectivity at relatively low reaction temperature ( $< 500^\circ\text{C}$ ), resulting in high ethylene yield ( $> 60\%$ ) [5,24]. Despite the advantages of the ODHE process and the high ethylene yield of MoVTeNb mixed oxide catalyst, the process has not been commercialized yet. For commercial implementation, several key requirements should be simultaneously satisfied: ethylene selectivity ( $> 90\%$ ), long-term stability, and ethylene productivity ( $> 1.0 \text{ kgC}_2\text{H}_4/\text{kg}_{\text{cat}} \text{ h}$ ) [4,25]. However, the requirements are restrictedly and/or partially satisfied by most conventional catalysts. Especially, such high criteria of ethylene productivity have been considered as major obstacle for commercialization of the process.

\* Corresponding author.

E-mail address: [jyi@snu.ac.kr](mailto:jyi@snu.ac.kr) (J. Yi).

<sup>1</sup> These authors contributed equally to this work.

There have been various attempts to improve the ethylene productivity using MoVTeNb-based mixed oxide catalysts. For example, supports such as  $\text{Al}_2\text{O}_3$ ,  $\text{SiO}_2$ , and  $\text{CeO}_2$  [13,26,27], post treatments [25], size control [6], and the introduction of additives [28,29] are used. Unfortunately, the ethylene productivity of them is still lower than the industrial criteria for the commercialization.

In this study, we developed Ce-incorporated MoVTeNbO catalysts for the production of ethylene via the ODHE reaction. Ce can be a proper hetero-atom as a dopant due to its high oxygen storage capacity and unique redox properties [30]. The active structure (*M1* phase) was maintained after Ce was incorporated into the MoVTeNbO framework, which was confirmed by XRD, TEM, STEM, Raman, and UV-vis DRS. DFT calculation results also provided an evidence for the incorporation of Ce into the framework. XPS and TPR analyses revealed that the incorporated Ce induced an abundance of  $\text{V}^{5+}$  species within the catalysts and an enhancement in reducibility of catalysts, which promotes conversion of ethane. In addition, it was confirmed that the amounts of available lattice oxygen to participate in the ODHE reaction became abundant in MoVTeNbCeO catalysts. The results of reaction tests proved that the catalytic activity was remarkably increased by the incorporation of Ce without losing its high ethylene selectivity. The catalytic performance was retained for 200 h with exhibiting commercially feasible ethylene productivity ( $1.11 \text{ kgC}_2\text{H}_4/\text{kg}_{\text{cat}} \text{ h}$ ). As far as we can ascertain, this is the first report developing a catalyst with the excellent ethylene productivity ( $> 1.00 \text{ kgC}_2\text{H}_4/\text{kg}_{\text{cat}} \text{ h}$ ), ethylene selectivity ( $> 94\%$ ), and long-term stability ( $> 200 \text{ h}$ ).

## 2. Methods

### 2.1. Catalyst preparation

MoVTeNbCeO catalysts were prepared by a hydrothermal method. A aqueous solution containing ammonium molybdate hydrate (10.07 g, 81.0–83.0%  $\text{MoO}_3$  basis, Sigma-Aldrich), 2.18 g of telluric acid (2.18 g, 99.0%, Sigma-Aldrich), cerium nitrate hexahydrate (0.50–3.00 g, 99%, Sigma-Aldrich), vanadium oxide sulfate hydrate (5.11 g, 97.0%, Sigma-Aldrich) with deionized water (58 mL) was prepared with vigorous stirring at 80 °C for 1 h (Solution 1). The color of mixture turned into green. Solution 2 was prepared with niobium oxide hydrate (1.22 g, CBMM), oxalic acid dehydrate (3.03 g, 99.0%, Sigma-Aldrich), deionized water (14 mL) at 80 °C for 30 min. The solutions were cooled down to room temperature. Then, solution 2 was added to solution 1, and the mixture was stirred for 30 min. The aqueous solution containing Mo, V, Te, Nb, and Ce precursors was heated at 175 °C for 48 h. The obtained precipitate was washed 3 times with deionized water by centrifugation (12,000 rpm), and dried overnight at 80 °C. The prepared samples were activated under inert atmosphere ( $\text{N}_2$ , 50 mL/min) at 600 °C for 2 h. The catalysts are denoted as MoVTeNbCeO-X where X indicates molar ratio of Ce to V in aqueous solution in preparation step. A reference sample (MoVTeNbO) was also prepared following previous procedure [31].

### 2.2. Characterization

XRD analysis was performed by a powder X-ray diffractometer (Rigaku d-MAX2500-PC,  $\text{CuK}_\alpha$  radiation, 50 kV, 100 mA). The morphology and lattice were characterized using a high-resolution transmission electron micrograph (HR-TEM) (JEOL JEM-3010, 300 kV). EDS chemical mapping images of the catalyst were obtained using Bright field scanning transmission microscopy (BF-STEM) (JEOL JEM-2100F). Ultraviolet-visible diffuse reflectance spectroscopy (UV-vis DRS) (Jasco V670 spectrometer) was conducted to obtain the spectra at room temperature. Raman shifts were collected using a HORIBA LabRAM HV Evolution (CCD detector, 532 nm of laser). The surface areas were measured on by a Micromeritics ASAP-2010 with  $\text{N}_2$  adsorption at  $-196^\circ\text{C}$ . Field emission electron probe microanalysis (EPMA) was

performed to investigate the elemental compositions (Mo, V, Te, Nb, Ce, and O) of the catalysts using JEOL JXA-8530F. X-ray photoelectron spectroscopy (XPS) spectra were recorded using AXIS SUPRA (Kratos). C 1s peak (284.5 eV) was used as a standard. Peak deconvolution for vanadium oxidation state ( $\text{V}^{4+}$  and  $\text{V}^{5+}$ ) was conducted based on previous researches [6].  $\text{H}_2$  temperature-programmed reduction ( $\text{H}_2\text{-TPR}$ ) was carried out by Micromeritics Autochem II chemisorption analyzer. The catalyst (0.1 g) was used in the analysis, and heated at 150 °C for 1 h under Ar flow. After that, it cooled to 50 °C. The gas flow was switched to 10%  $\text{H}_2/\text{Ar}$  flow (30 mL/min), and the temperature was then ramped from 50 °C to 800 °C at 10 °C/min. TCD detector was used to measure  $\text{H}_2$  consumption during ramping step.

Lattice oxygen capacity measurement was applied to investigate the lattice oxygen species of catalysts available for the reaction. The measurement was conducted in a flow reactor system with 6 port valves for the rapid introduction of an ethane pulse. 0.2 g of powders was placed on a quartz bed reactor (8 mm i.d.). He (26.6 mL/min) was used as a carrier gas. The signals of the outlet gas were detected by an on-line mass spectrometer (QGA, Hiden Analytical). Prior to the measurements, the samples were heated at 400 °C in  $\text{O}_2$  (2.4 mL/min) and He (26.6 mL/min) for 1 h. Then, the sample was purged in He for 30 min to remove residual oxygen from the system. 250  $\mu\text{L}$  of ethane was injected along with carrier gas (He) to the samples 12 times. Instantaneous ethane consumption was monitored as a function of time. Lattice oxygen capacity was calculated as micromoles of ethylene produced per gram of the sample.

### 2.3. Reaction test

A 0.2 g of catalyst was used for oxidative dehydrogenation of ethane using a quartz reactor (8 mm i.d.). Before the reaction, pre-heating step was carried out at 250 °C under an inert flow (He: 39.2 mL/min and  $\text{N}_2$ : 16.3 mL/min) for 1 h. Then,  $\text{O}_2$  and ethane was introduced. The molar composition of feed mixture was  $[\text{Ethane}/\text{O}_2/\text{N}_2/\text{He}] = [5.0/2.5/27.2/65.3]$ .  $\text{N}_2$  was used as internal standard for analyzing the gas-phase products. Due to the induction time for ODHE reaction, reaction data were collected at 6 h. The products were analyzed by an online GC (Younglin ACME 6100 model) equipped with both a flame ionization detector (FID) and a thermal conductivity detector (TCD). Two columns were used in the analysis (Porapak Q for  $\text{CO}_2$ ,  $\text{C}_2\text{H}_4$ ,  $\text{C}_2\text{H}_6$  and Molsieve 13X for  $\text{N}_2$ ,  $\text{O}_2$ , CO. Ethane conversion, ethylene yield, selectivity, and productivity, and  $\text{CO}_x$  selectivity were calculated as follows:

$$\text{Ethane conversion (\%)} = \frac{\text{mole of ethane reacted}}{\text{mole of ethane fed}} \times 100$$

$$\text{Ethylene yield (\%)} = \frac{\text{mole of ethylene produced}}{\text{mole of ethane fed}} \times 100$$

$$\text{Ethylene Selectivity (\%)} = \frac{\text{mole of ethylene produced}}{\text{mole of ethane reacted}} \times 100$$

$$\text{CO}_x \text{ Selectivity (\%)} = \frac{\text{mole of CO}_x \text{ produced}}{\text{mole of ethane reacted}} \times \frac{1}{2} \times 100$$

$$\text{Ethylene productivity (kgC}_2\text{H}_4/\text{kg}_{\text{cat}} \cdot \text{h}) = \frac{\text{F}_{\text{C}_2\text{H}_6} \cdot \text{X}_{\text{C}_2\text{H}_6} \cdot \text{S}_{\text{C}_2\text{H}_4} \cdot \text{MW}_{\text{C}_2\text{H}_4}}{\text{m}_{\text{cat}}}$$

where  $\text{F}_{\text{C}_2\text{H}_6}$  is the molar flow of ethane,  $\text{X}_{\text{C}_2\text{H}_6}$  is conversion of ethane,  $\text{S}_{\text{C}_2\text{H}_4}$  is selectivity to ethylene,  $\text{MW}_{\text{C}_2\text{H}_4}$  is molecular weight of ethylene (28.05 g/mol), and  $\text{m}_{\text{cat}}$  is the mass of the catalyst. The carbon balance was closed to 100% for each run.

### 2.4. DFT calculations

Density functional theory (DFT) calculations were performed by The Vienna Ab-initio Simulation Package (VASP) [32]. For exchange-correlation functional, the Perdew–Burke–Ernzerhof (PBE) of the

generalized gradient approximation (GGA) was used [33]. Electron-ion interactions were described using the projector augmented wave (PAW) method [34]. The energy cutoff was 520 eV and the integration of the Brillouin zone was performed  $1 \times 1 \times 5$  Monkhorst-Pack k-point sampling. The convergence criteria were set to  $2 \times 10^{-8}$  eV and  $3 \times 10^{-2}$  eV/Å for energy and force, respectively.

Incorporation energy of Ce into Mo sites ( $E_{\text{Incorporation-Mo}}$ ) and hollow site ( $E_{\text{Incorporation-Hollow}}$ ) was calculated by following equations.

$$E_{\text{Incorporation-Mo}} = (E_{\text{Ce}} \text{ incor-MoVTeNbO} + E_{\text{Mo}}) - (E_{\text{MoVTeNbO}} + E_{\text{Ce}})$$

$$E_{\text{Incorporation-Hollow}} = (E_{\text{Ce}} \text{ hollow-MoVTeNbO}) - (E_{\text{MoVTeNbO}} + E_{\text{Ce}})$$

where  $E_{\text{Ce}} \text{ incor-MoVTeNbO}$  is the bulk energy of MoVTeNbO unit cell in which Ce atom is incorporated into Mo atom site,  $E_{\text{Mo}}$  is the bulk energy of the Mo metal per atom,  $E_{\text{MoVTeNbO}}$  is the bulk energy of MoVTeNbO unit cell,  $E_{\text{Ce}}$  is the bulk energy of the Ce metal per atom, and  $E_{\text{Ce}} \text{ hollow-MoVTeNbO}$  is the bulk energy of MoVTeNbO unit cell in which Ce atom is incorporated into hollow site.

### 3. Results and discussion

#### 3.1. Structural characterizations of MoVTeNbCeO catalysts

The compositional ratios of the catalysts were confirmed using electron probe micro-analyzer (EPMA), as shown in Table 1. Ce was detected in all MoVTeNbCeO samples, and the content was increased in the catalysts as the amount of Ce precursor in preparation solutions was increased. The compositions of Mo and V were gradually decreased and increased, respectively, while those of Te and Nb were well maintained as the fraction of Ce was increased. An abrupt increase in Ce concentration of MoVTeNbCeO-0.3 can be attributed to the formation of a different phase.

The crystalline structures of the MoVTeNbO and MoVTeNbCeO catalysts were investigated by XRD analysis in Fig. 1. The content of Ce atoms was varied with 0.05, 0.07, 0.1, 0.15, 0.2, and 0.3 in MoVTeNbCeO samples. The corresponding peaks of both the M1 phase (6.5°, 7.8°, 8.9°, 22.0°, 27.1°, 35.0°, and 45.0°: PDF 00-058-0789) and the M2 phase (22.0°, 28.3°, 36.1°, 45.0°, 50.1°, 53.9°, 55.4°, and 58.7°: PDF 00-057-1099) were observed simultaneously for MoVTeNbO sample. It should be noted that the M1 phase is the active structure for ethylene production via the ODHE reaction [14,27]. After the addition of Ce, the crystalline structures (M1 and M2 phases) were retained (Fig. 1b–f) without peaks corresponding for  $\text{CeO}_x$  species. The orderedness of a-b plane (6.5°, 7.8°, 8.9°, 22.0°, and 45.0°) and c-direction (22.0° and 27.1°) for M1 phase was well preserved despite the incorporation of Ce. These results show that MoVTeNbCeO catalysts could be active for the ODHE reaction. Intensity of the peaks attributed to the M2 phase was increase as the incorporated amount of Ce was increased from MoVTeNbO to MoVTeNbCeO-0.2, indicating incorporated Ce could encourage to form M2 phase. When the ratio of Ce to V became 0.3, the

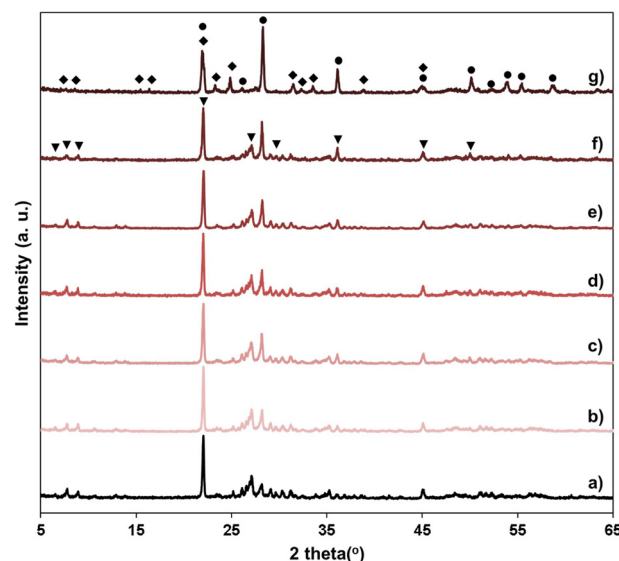


**Fig. 1.** XRD patterns of MoVTeNbO and MoVTeNbCeO with different Ce contents: a) MoVTeNbO, b) MoVTeNbCeO-0.05, c) MoVTeNbCeO-0.07, d) MoVTeNbCeO-0.1, e) MoVTeNbCeO-0.15, f) MoVTeNbCeO-0.2, and g) MoVTeNbCeO-0.3 catalysts. ▼: PDF 00-058-0789 (M1 phase), ●: PDF 00-057-1099 (M2 phase), ◆: PDF 00-058-0788 (( $\text{Mo}_{0.6}\text{Nb}_{0.22}\text{V}_{0.18}$ )<sub>5</sub>O<sub>14</sub>).

catalyst exhibited a new phase (7.7°, 8.6°, 15.5°, 16.4°, 22.1°, 23.3°, 24.9°, 31.5°, 32.3°, 33.5°, 38.9°, and 45.0°: PDF 00-058-0788, ( $\text{Mo}_{0.6}\text{Nb}_{0.22}\text{V}_{0.18}$ )<sub>5</sub>O<sub>14</sub>) with the M2 phase and lost the M1 phase. Due to degradation of M1 phase and formation of the inactive phase, no catalytic activity for MoVTeNbCeO-0.3 could be observed.

The lattice parameter and the cell volume were calculated based on the XRD patterns before and after the incorporation of Ce, as shown in Table 1. The results show that values for both lattice parameter and cell volume tended to increase with an increase in the amount of Ce atoms in MoVTeNbCeO. The atomic radius of Ce ions is larger than those of the host metal cations (e.g., Mo, V, Te, and Nb), which may lead to an enlargement of the lattice parameter and to an expansion of cell volume. These results provide further evidence that the Ce atoms were incorporated in the MoVTeNbO framework. DFT calculations (See DFT modeling section in the Supporting information: Figs. S1 and S2, and Table S1) also proved that the incorporation of Ce caused an enlargement of the lattice parameters (Table 2). This is in good agreement with the results calculated from the XRD patterns.

TEM images of MoVTeNbO and MoVTeNbCeO samples except MoVTeNbCeO-0.3 shows the particle shapes had rod-like features with an average diameter in ranges of 40–60 nm (Fig. 2a–f). Due to the similar shape of the catalysts, the differences in the surface area were negligibly low, less than  $2 \text{ m}^2/\text{g}$ . (Table 1). It was confirmed that the

**Table 1**

Physicochemical properties of MoVTeNbO and MoVTeNbCeO samples with various Ce contents.

	Surface area <sup>a</sup> ( $\text{m}^2/\text{g}$ )	Composition <sup>b</sup> (%)	Lattice parameters <sup>c</sup> (Å)			Cell volume <sup>c</sup> (Å <sup>3</sup> )
			a	b	c	
MoVTeNbO	9.5	22.26/5.52/3.10/2.48/0.00/66.61	21.1289	26.5744	4.0189	2256.55
MoVTeNbCeO-0.05	9.8	21.51/6.04/3.09/2.46/0.16/66.74	21.1477	26.5800	4.0162	2257.53
MoVTeNbCeO-0.07	9.7	21.53/6.13/3.10/2.35/0.20/66.69	21.1515	26.6057	4.0158	2259.89
MoVTeNbCeO-0.1	10.4	21.48/6.42/3.13/2.28/0.28/66.41	21.1580	26.5662	4.0221	2260.77
MoVTeNbCeO-0.15	10.6	21.46/6.64/3.08/2.26/0.39/66.17	21.1370	26.6488	4.0172	2262.79
MoVTeNbCeO-0.2	11.9	21.49/6.92/3.07/2.29/0.59/65.63	21.1656	26.5779	4.0277	2265.73
MoVTeNbCeO-0.3	6.7	21.26/6.15/2.72/2.38/1.38/66.11	–	–	–	–

<sup>a</sup> Specific surface areas were determined from the  $\text{N}_2$  adsorption branch.

<sup>b</sup> Compositions of the catalysts were measured by EPMA.

<sup>c</sup> Lattice parameters and cell volumes for the M1 phase were calculated by fitting XRD patterns based on the M1 phase (PDF 00-058-0789).

**Table 2**

DFT-calculated lattice parameters of MoVTeNbO and MoVTeNbCeO models.

Model	Lattice parameter (Å)		
	a	b	c
MoVTeNbO	21.2069	26.9136	4.1471
MoVTeNbCeO	21.3019	26.9567	4.1618

unique lattice structure (layered structure) for MoVTeNbCeO-0.05 to MoVTeNbCeO-0.2 was observed (Fig. 2b–f), which was identical to that for MoVTeNbO. Other lattice structures such as CeO<sub>x</sub> were out of observation. On the contrary, MoVTeNbCeO-0.3 sample showed irregular shape and different lattice structure from the other samples (Fig. 2g). The different SAED pattern of MoVTeNbCeO-0.3 sample from the other samples was ascribed to the change in phase. Also, other patterns originated from CeO<sub>x</sub> were not detected in the SAED patterns of the catalysts [35,36]. These results are consistent with the results obtained from XRD analysis.

For further verification of the incorporation of Ce atoms, EDS elemental mapping images were obtained for MoVTeNbCeO catalysts, as shown in Figs. 3 and S3. The results show that all components (Mo, V, Te, Nb, and Ce) were highly distributed within the samples. The highly dispersed Ce atoms revealed the absence of CeO<sub>x</sub> particles. It can be an additional evidence that Ce atoms are incorporated into the MoVTeNbO framework. Even for MoVTeNbCeO-0.3, which exhibits different phase from other samples, high dispersion of Ce species was observed.

Fig. S4 shows Raman spectra of MoVTeNbO and MoVTeNbCeO samples including reference material, CeO<sub>2</sub>. As confirmed by XRD analysis, peaks corresponding to M1 (450, 820, and 874 cm<sup>-1</sup>) and M2 (440, 796, and 874 cm<sup>-1</sup>) phases were observed for the pristine catalyst [14]. The spectra of MoVTeNbCeO-0.05 to MoVTeNbCeO-0.2 were

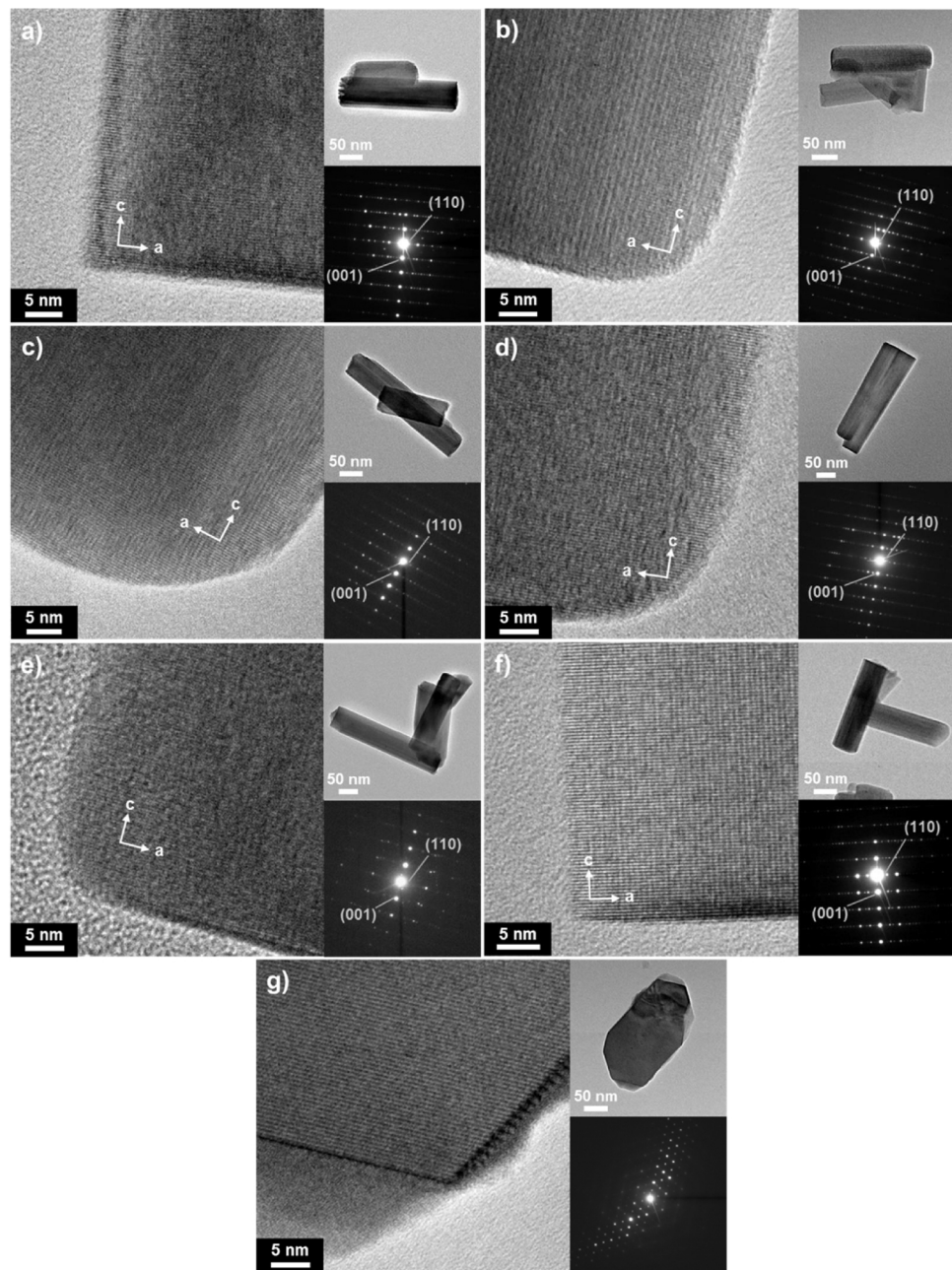


**Fig. 2.** TEM images and corresponding selected area electron diffraction (SAED) patterns of a) MoVTeNbO, b) MoVTeNbCeO-0.05, c) MoVTeNbCeO-0.07, d) MoVTeNbCeO-0.1, e) MoVTeNbCeO-0.15, f) MoVTeNbCeO-0.2, and g) MoVTeNbCeO-0.3 catalysts.

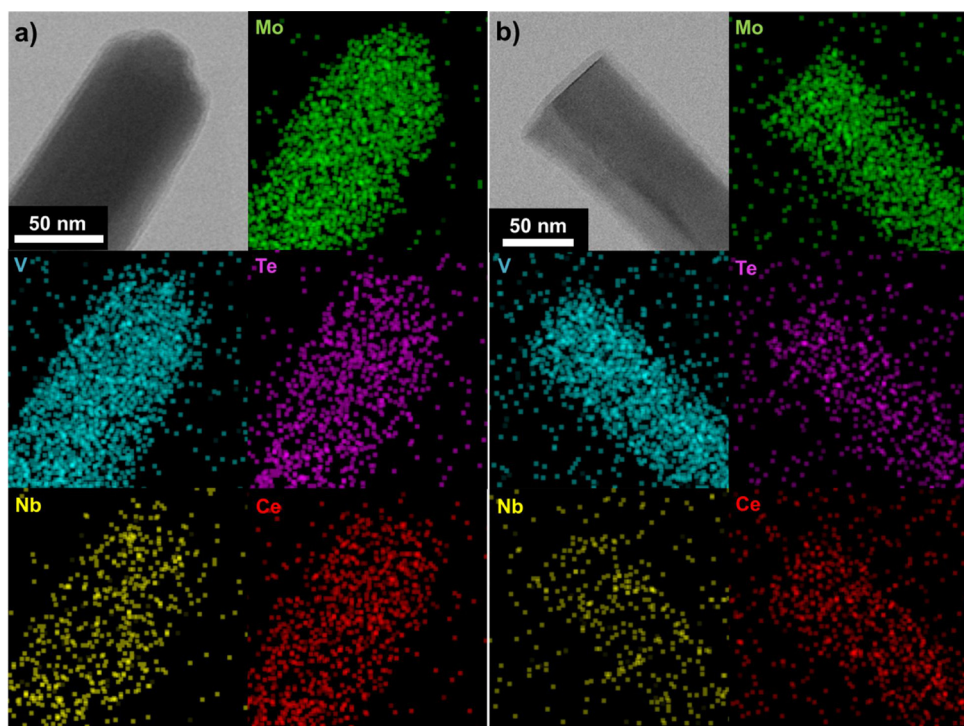


Fig. 3. Bright field STEM images of a) MoVTeNbCeO-0.05, b) MoVTeNbCeO-0.1, and corresponding elemental mapping images of Mo, V, Te, Nb, and Ce.

similar to that of MoVTeNbO. The only difference is peak intensity corresponding to the *M1* phase. Distinct peak corresponding to *M1* phase was observed for MoVTeNbO sample at  $820\text{ cm}^{-1}$ . As the content of Ce was increased, its intensity was decreased from MoVTeNbCeO-0.05 to MoVTeNbCeO-0.2 samples. After all, the peak disappeared when the Ce ratio reached 0.3, which is good agreement with XRD pattern. No peak corresponding to  $\text{CeO}_2$  was detected in the Raman spectra of MoVTeNbCeO catalysts.

In UV-vis DRS spectra of all samples (Fig. S5), the broad bands in the region of 250–450 nm are related to the presence of  $\text{Te}^{6+}$ ,  $\text{Mo}^{6+}$ ,  $\text{V}^{5+}$ , and  $\text{Nb}^{5+}$  [37,38]. Similar shape of spectra for MoVTeNbCeO-0.05 to MoVTeNbCeO-0.2 was observed to that of MoVTeNbO sample. The significant band broadening of MoVTeNbCeO-0.3 indicates the presence of structural distortion, as XRD and TEM results.

XPS spectra of Ce 3d showed that most of the incorporated Ce atoms were of presence in  $\text{Ce}^{3+}$  rather than  $\text{Ce}^{4+}$  (Fig. S6) [39,40]. Considering that  $\text{CeO}_2$  exhibits characteristic peak at 916.4 eV [40], it could imply the absence of  $\text{CeO}_2$  particles deposited on the surface of MoVTeNbCeO catalysts. From the result, it was expected that incorporation of Ce into the framework rather than deposition of  $\text{CeO}_2$  species on the framework.

### 3.2. Effects of incorporated Ce on the reducibility and oxidation state of V in the catalysts

Fig. 4 shows the TPR spectra of MoVTeNbO and MoVTeNbCeO samples. Broad peak in a range from 450 to 650 °C was obtained for the samples where *M1* phase are present. This is a typical shape in the TPR spectrum of a MoVTeNbO catalyst, which originated from the reduction of metal cations [6,41]. The different spectrum of MoVTeNbCeO-0.3 from that of the others indicates a different phase of the catalyst. It was noteworthy that the peak was shifted to a lower temperature when Ce was incorporated to MoVTeNbO framework except MoVTeNbCeO-0.3. This indicates that nature of the lattice oxygen was changed by incorporation of Ce. It can be ascribed to incorporated Ce enhancing reducibility of the catalyst, which resulted in the easier migration of oxygen species from bulk to surface and the generation of reactive oxygen species [42].

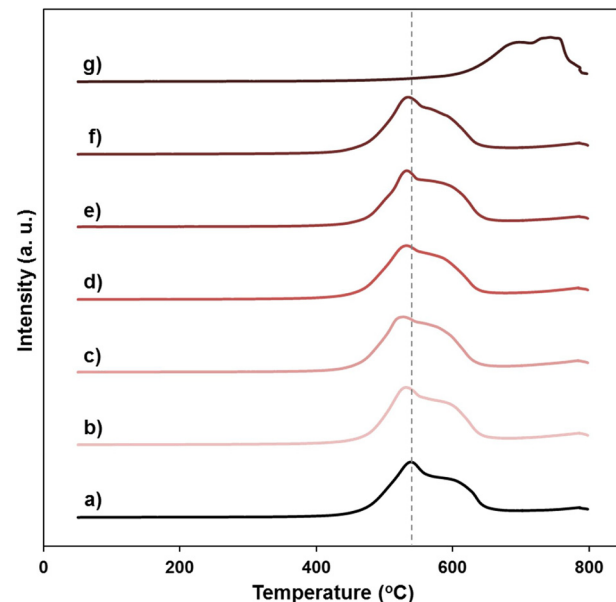


Fig. 4. TPR spectra of MoVTeNbO and MoVTeNbCeO with various Ce contents: a) MoVTeNbO, b) MoVTeNbCeO-0.05, c) MoVTeNbCeO-0.07, d) MoVTeNbCeO-0.1, e) MoVTeNbCeO-0.15, f) MoVTeNbCeO-0.2, and g) MoVTeNbCeO-0.3 catalysts.

XPS analysis was conducted to reveal the influence of incorporated Ce on oxidation state of V in the catalysts. According to previous reports, the oxidation state of V is the determining factor for the conversion of ethane [6,27]. The fraction of  $\text{V}^{5+}$  was increased when Ce was incorporated into MoVTeNbO framework (Table 3 and Fig. 5). This means that incorporated Ce induced  $\text{V}^{5+}$  rather than  $\text{V}^{4+}$ . In detail, the ratio of  $\text{V}^{5+}$  to  $\text{V}^{4+}$  was gradually increased from 0.542 for MoVTeNbO to 0.761 for MoVTeNbCeO-0.1, and decreased to 0.614 for MoVTeNbCeO-0.2. The abundance of  $\text{V}^{5+}$  rather than  $\text{V}^{4+}$  can lead to a positive effect on the catalytic activity of MoVTeNbCeO.

**Table 3**

Oxidation state of vanadium in MoVTeNbO and MoVTeNbCeO samples with various Ce contents.

Sample	$V^{5+}/V^{4+}$
MoVTeNbO	0.542
MoVTeNbCeO-0.05	0.677
MoVTeNbCeO-0.07	0.702
MoVTeNbCeO-0.1	0.761
MoVTeNbCeO-0.15	0.703
MoVTeNbCeO-0.2	0.614
MoVTeNbCeO-0.3	0.681

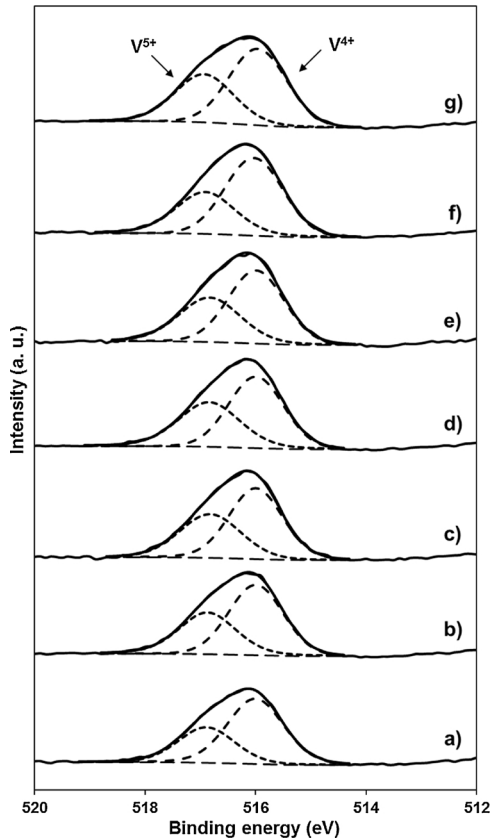


**Fig. 5.** XPS spectra of V 2p<sub>3/2</sub> for MoVTeNbO and MoVTeNbCeO with various Ce contents: a) MoVTeNbO, b) MoVTeNbCeO-0.05, c) MoVTeNbCeO-0.07, d) MoVTeNbCeO-0.1, e) MoVTeNbCeO-0.15, f) MoVTeNbCeO-0.2, and g) MoVTeNbCeO-0.3 catalysts.

### 3.3. Effects of incorporated Ce on catalytic activity for oxidative dehydrogenation of ethane

The reaction parameters were optimized for the oxidative dehydrogenation of ethane: reaction temperature, feed flow rate, and feed ratio (O<sub>2</sub>/C<sub>2</sub>H<sub>6</sub>). The MoVTeNbCeO-0.1 sample was tested for the optimization process. Fig. S7 shows the results of the catalytic test at different reaction temperatures. The level of ethane conversion was gradually increased up to 475 °C. When the temperature reached 500 °C, the ethane conversion was slightly decreased from 59.9 to 57.9%. This can be caused by a partial degradation of the active M1 phase, and formation of inactive MoO<sub>2</sub> phase due to high reaction temperature in reaction steam (Fig. S8). Byproducts (CO and CO<sub>2</sub>) were observed at 400 °C. Their productions and O<sub>2</sub> conversion were increased with increase in temperatures up to 14.4% and 81.8%, respectively. The results could be originated from unselective oxidation caused by reactive O<sub>2</sub> at high temperature. Therefore, 425 °C was determined to be the optimum temperature for the production of ethylene at a yield of 54.3%.

The variations in catalytic performances were investigated according to flow rates in a range from 20 to 80 mL/min, as shown in Fig. S9. A total feed flow rate of 60 mL/min was chosen as optimal based on the highest ethylene yield within the tested range of flow rates. The conversion of ethane and O<sub>2</sub> was suppressed under 80 mL/min of flow rate due to insufficient contact time between the reactants and the catalyst. On the contrary, a low feed flow rate leads to a re-adsorption of ethylene, and an over-oxidation of the ethane and as-produced ethylene, which promoted complete oxidation. Consequently, high fractions (40.8%) of CO and CO<sub>2</sub> in products were detected with significant decline in ethylene selectivity to below 60%.

The feed ratio between ethane and O<sub>2</sub> is considered as one of the important factor to determine ethane activity and ethylene selectivity. The ethane conversion activity was increased with increases in the ratio of O<sub>2</sub>/ethane, and ethylene selectivity was simultaneously decreased (Fig. S10). Abundant oxygen species in the feed not only accelerated the conversion of ethane but also promote the total oxidation, which resulted in a decrease in ethylene selectivity. Although the yield of ethylene reached ~60% at O<sub>2</sub>:ethane ratios of 1.5:2 and 2:2, the ratio of 1:2 was chosen as the optimum point due to higher levels of ethylene selectivity (95.5%) compared to those (< 85%) at O<sub>2</sub>:ethane ratios of 1.5:2 and 2:2.

To investigate the effect of incorporated Ce on catalytic performance, reaction tests were conducted for both MoVTeNbO and MoVTeNbCeO with various amount of Ce (Fig. 6). The bare sample exhibited an ethane conversion of 38.8% and ethylene selectivity of 94.1%, leading to an ethylene yield of 36.5%. When Ce was incorporated into MoVTeNbO framework, the activity of MoVTeNbCeO-0.05 (48.0%) and MoVTeNbCeO-0.07 (50.5%) was enhanced compared to that of MoVTeNbO while the selectivity for ethylene was maintained with a high level (~95%). For MoVTeNbCeO-0.1, the highest ethylene yield (54.3%) was obtained among the prepared samples without losing its ethylene selectivity (95.5%). Considering similarities of the physicochemical properties (surface area, crystalline structure, and shape of catalyst) of MoVTeNbO and MoVTeNbCeO-0.1 catalysts, the high production of ethylene over MoVTeNbCeO-0.1 was attributed to the enhanced reducibility and the abundance of V<sup>5+</sup> caused by incorporating Ce into the framework. In addition, considering that byproducts (e.g., CO<sub>2</sub>) are produced when ethane reacts with O<sup>2-</sup> whereas ethylene is produced when ethane reacts with lattice O<sup>2-</sup> [16], it is suggested that the incorporation of Ce atoms contributed to the selective formation of O<sup>2-</sup> rather than electrophilic O<sup>2-</sup> species. As the content of Ce was increased from 0.1 to 0.2 via 0.15, ethane conversion and ethylene yield were gradually decreased to less than those for MoVTeNbCeO-0.05. Contrary to other MoVTeNbCeO catalysts, MoVTeNbCeO-0.3 showed no activity for the oxidative dehydrogenation of ethane. This is because of the degradation of the active phase (M1 phase), which was confirmed via XRD, TEM, Raman, and UV-vis DRS.

For the clear comparison between incorporated Ce atom into the framework and loaded Ce species on the surface, we prepared 0.28 at.% (0.97 wt.%) Ce/MoVTeNbO, as a control sample, by incipient wetness impregnation method. The value of 0.28 at.% for Ce is the same concentration with that of MoVTeNbCeO-0.1 (Table 1). Surface compositions of MoVTeNbO, MoVTeNbCeO, and 0.28 at.% Ce/MoVTeNbO samples, especially Ce, were measured by XPS (Table S2). Relatively low Ce concentration on the surface of MoVTeNbCeO catalysts was observed compared to that in bulk of the catalysts (Table 1). In addition, it was confirmed that Ce content on the surface of 0.28 at.% Ce/MoVTeNbO was 4.7 times higher than that on the surface of MoVTeNbCeO-0.1 although they had the same amount of Ce in bulk. This indicates that Ce atoms were incorporated into MoVTeNbO framework rather than deposited on the surface for MoVTeNbCeO catalysts. In the reaction tests, it was shown that the catalytic activity for 0.28 at.% Ce/MoVTeNbO was lower than that for Ce-incorporated MoVTeNbO catalyst, even than that for bare MoVTeNbO catalyst (Figs. S11 and Fig. 6). Linear decrease in O<sub>2</sub> conversion (63.2% to 25.9%) with ethane

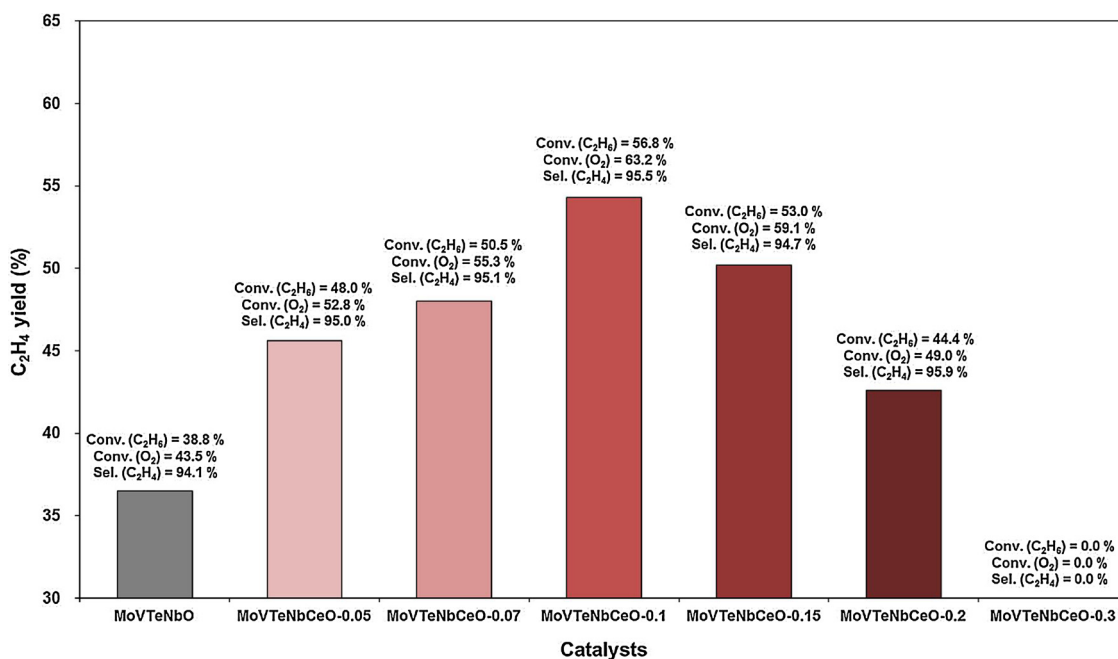


**Fig. 6.** Reaction results for the oxidative dehydrogenation of ethane over MoVTeNbO and MoVTeNbCeO with various Ce contents. 0.2 g of catalyst, 60 mL/min of total flow,  $\text{O}_2:\text{C}_2\text{H}_6$  ratio = 1:2, 5 vol.% of  $\text{C}_2\text{H}_6$ , 425 °C of reaction temperature.

conversion (58.8% to 20.3%) suggested no promotion effect was induced by the loaded Ce species on the catalyst surface, such as promotion of  $\text{O}_2$  evolution. The decrease in the catalytic activity for 0.28 at.-%Ce/MoVTeNbO can be ascribed to the covering of catalytically low-active Ce oxide species (see Fig. S12) on the surface active site of MoVTeNbO. These characterization and reaction results can be an evidence for incorporation of Ce into MoVTeNbO framework rather than deposition on the surface, inducing change in chemical properties.

The ODHE reaction pathway over MoVTeNbO catalyst is known to follow the Mars-van Krevelen mechanism [12,41]. The reaction is initiated at the C–H group of an ethane molecule that is activated by the surface lattice oxygen in the catalyst. Ethylene is then detached from the surface and the remaining hydroxyl groups form water. Reduced species are re-oxidized by gas phase  $\text{O}_2$ . Therefore, it is reasonable that the catalytic activity has a relation with the amount of the lattice oxygen. In order to measure the quantity of the available lattice oxygen species for the MoVTeNbO and MoVTeNbCeO samples, we performed the pulse injection method, and the results are listed in Table 4. We found that the amount of lattice oxygen was increased after the incorporation of Ce atoms. The measured lattice oxygen capacity was in the order of MoVTeNbO (29.6  $\mu\text{mol/g}_{\text{cat}}$ ) < MoVTeNbCeO-0.05 (32.2  $\mu\text{mol/g}_{\text{cat}}$ ) < MoVTeNbCeO-0.2 (35.3  $\mu\text{mol/g}_{\text{cat}}$ ) < MoVTeNbCeO-0.07 (39.9  $\mu\text{mol/g}_{\text{cat}}$ ) < MoVTeNbCeO-0.15 (42.2  $\mu\text{mol/g}_{\text{cat}}$ ) < MoVTeNbCeO-0.1 (47.0  $\mu\text{mol/g}_{\text{cat}}$ ). It should be noted that MoVTeNbCeO-0.1 catalyst had the largest amount of lattice oxygen, which was 1.6 times greater amount than that of the MoVTeNbO

sample. This result indicates that the proper amount of incorporated Ce atoms tunes the metal–oxygen bonding properties, which allows generation of available lattice oxygen species to ODHE reaction. The correlation plot between lattice oxygen capacity and ethylene yield reveals that the quantity of lattice oxygen available to ODHE reaction has relations with the catalytic performance (Fig. 7).

In addition to lattice oxygen capacity, it is well-known that  $\text{V}^{5+}$  is an important factor in catalytic activity [6,27]. The highest catalytic performance of MoVTeNbCeO-0.1 was originated from the highest concentration of  $\text{V}^{5+}$  species as well as from the largest capacity for lattice oxygen among the catalysts (see Table 3). In Fig. 6, MoVTeNbCeO-0.05 exhibited higher activity than MoVTeNbCeO-0.2, although MoVTeNbCeO-0.05 had lower lattice oxygen capacity compared to MoVTeNbCeO-0.2. It is because higher fraction of  $\text{V}^{5+}$  for MoVTeNbCeO-0.05 encouraged conversion of ethane compared to that for MoVTeNbCeO-0.2. In case of MoVTeNbCeO-0.07 and MoVTeNbCeO-0.15, although similar fractions of  $\text{V}^{5+}$  were observed, higher ethylene yield of MoVTeNbCeO-0.15 was observed than that of MoVTeNbCeO-0.07. It can come from larger lattice oxygen capacity (42.2  $\mu\text{mol/g}_{\text{cat}}$ ) of

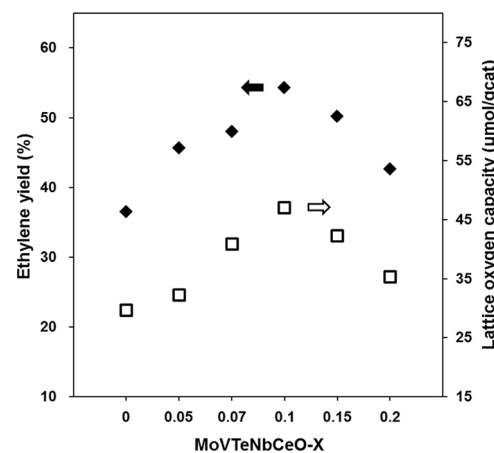


**Fig. 7.** Correlation of ethylene yield and lattice oxygen capacity as a function of Ce contents of MoVTeNbO and MoVTeNbCeO catalysts.

**Table 4**

Lattice oxygen capacity of MoVTeNbO and MoVTeNbCeO with various Ce contents measured by pulse injection method.

Sample	Lattice oxygen capacity ( $\mu\text{mol/g}_{\text{cat}}$ )
MoVTeNbO	29.6
MoVTeNbCeO-0.05	32.2
MoVTeNbCeO-0.07	39.9
MoVTeNbCeO-0.1	47.0
MoVTeNbCeO-0.15	42.2
MoVTeNbCeO-0.2	35.3
MoVTeNbCeO-0.3	–

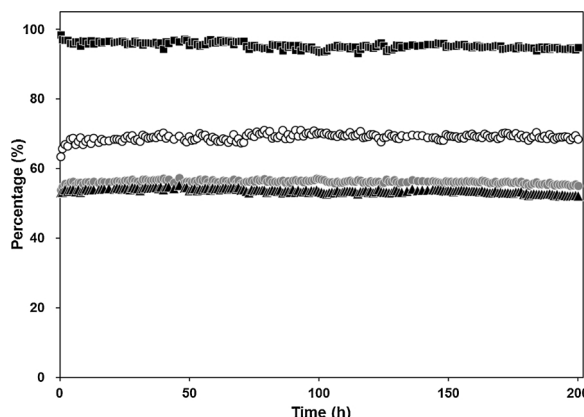


**Fig. 8.** Long-term test for MoVTeNbCeO-0.1 catalyst. 0.2 g of catalyst, 60 mL/min of total flow.  $[O_2 : C_2H_6 : He + N_2] = [5:10:85]$  in Vol.%, 400 °C of reaction temperature. ●: ethane conversion, ○:  $O_2$  conversion, ■: ethylene selectivity, ▲: ethylene yield.

MoVTeNbCeO-0.15 than that ( $39.9 \mu\text{mol/g}_{\text{cat}}$ ) of MoVTeNbCeO-0.07. Based on the comparisons, it was confirmed that both of the abundance of  $V^{5+}$  and large lattice oxygen capacity are determining factors to catalytic activity for ODHE reaction.

As previously mentioned, for the commercialization of the ODHE process, a catalyst should exhibit high ethylene selectivity (> 90%), ethylene productivity (>  $1.0 \text{ kgC}_2\text{H}_4/\text{kg}_{\text{cat}} \text{ h}$ ), and catalytic stability simultaneously [4,25]. To check the commercial applicability of the catalyst, the catalytic test over MoVTeNbCeO-0.1 with a 10% ethane feed stream was carried out at optimal and safe reaction condition (Fig. 8, and Tables S3 and S4). At the early stage (< 5 h) of the test, the catalyst was activated under reaction stream, resulting in slight increase in ethane and  $O_2$  conversions, and decrease in ethylene selectivity (Table S5). And then, the catalytic performance of the sample was retained to the value in steady-state (ethane conversion > 55%,  $O_2$  conversion  $\approx 69\%$ , ethylene selectivity > 94%) for 200 h. The phenomenon is related with the features of M1 phase catalyst, which is more active and selective when it activated under neutral or reducing atmosphere than under oxidizing one (Figs. S13–S15) [43]. In other words, reactants can allow the catalyst to be active and stable during reaction rather than to be deactivated. From this, long exchange cycle of catalysts, and avoidance of activity deactivation during reaction can be expected in an industrial aspect. Based on the ethane conversion and ethylene selectivity in long-term test, the ethylene productivity was calculated to be  $1.11 \text{ kgC}_2\text{H}_4/\text{kg}_{\text{cat}} \text{ h}$ . Such a high productivity with high ethylene selectivity (> 90%) was rarely achieved by the previously reported catalysts (see Table S6 in Supporting information). In addition, the active phase (M1) was well maintained after the test, which was confirmed by the XRD analysis (Fig. S16). Consequently, we proved the MoVTeNbCeO catalyst exhibits high ethylene productivity ( $1.11 \text{ kgC}_2\text{H}_4/\text{kg}_{\text{cat}} \text{ h}$ ) with high ethylene selectivity (> 94%) and long-term stability ( $\sim 200$  h) at low temperature (400 °C), and this result can be a step forward for the industrial ODHE process.

#### 4. Conclusions

Promotion effect of Ce in MoVTeNbCeO catalyst on catalytic activity of oxidative dehydrogenation of ethane to ethylene was studied. From XRD analysis and DFT calculations, a lattice expansion of MoVTeNbO framework for MoVTeNbCeO catalysts was obtained, which is an evidence of incorporation of Ce into the framework. In addition to XRD analysis, TEM, Raman, and UV-vis DRS spectroscopies revealed the maintenance of the unique structure of MoVTeNbO, which is active phase for ODHE, after Ce was inserted to the framework. TPR and pulse injection analyses indicate that the presence of Ce in MoVTeNbO

structure enhanced the reducibility of the catalysts and enriched the available lattice oxygen species for ODHE reaction. It was observed that the incorporated Ce atoms induced a high oxidation state in the V atoms ( $V^{5+}$  rather than  $V^{4+}$ ). These properties promote the conversion of ethane. Accordingly, MoVTeNbCeO catalysts exhibited higher activity (up to 56.8%) for ODHE than MoVTeNbO catalyst (38.8%) without losing selectivity to ethylene (> 95.0%). Especially, MoVTeNbCeO-0.1 catalyst showed the highest ethylene yield (54.3%) due to its high fraction of  $V^{5+}$  and large amount of lattice oxygen with the enhancement in reducibility. In long-term test, the catalyst showed high stability for 200 h while maintaining a high ethylene productivity ( $1.11 \text{ kgC}_2\text{H}_4/\text{kg}_{\text{cat}} \text{ h}$ ) and 95.4% of ethylene selectivity. It is suggested that MoVTeNbCeO catalyst exhibited the economically feasible productivity of ethylene with long-term stability.

#### Acknowledgments

This work was supported by the Center for C1 Gas Refinery grant funded by the Korean government (Ministry of Science, ICT & Future Planning, NRF-2016M3D3A1A01913255). This research was supported by the Supercomputing Center/Korea Institute of Science and Technology Information with supercomputing resources that included technical support (KSC-2016-C2-0024).

#### Appendix A. Supplementary data

Supplementary material related to this article can be found, in the online version, at doi:<https://doi.org/10.1016/j.apcatb.2018.06.025>.

#### References

- [1] H. Zhu, D.C. Rosenfeld, M. Harb, D.H. Anjum, M.N. Hedhili, S. Ould-Chikh, J.-M. Basset,  $Ni-M-O$  ( $M = Sn, Ti, W$ ) catalysts prepared by a dry mixing method for oxidative dehydrogenation of ethane, *ACS Catal.* 6 (2016) 2852–2866.
- [2] S. Yusuf, L.M. Neal, F. Li, Effect of promoters on manganese-containing mixed metal oxides for oxidative dehydrogenation of ethane via a cyclic redox scheme, *ACS Catal.* 7 (2017) 5163–5173.
- [3] B. Sarkar, R. Goyal, L.N. Konathala, C. Pendem, T. Sasaki, R. Bal, *Appl. Catal. B: Environ.* 217 (2017) 637–649.
- [4] F. Cavani, N. Ballarini, A. Cericola, Oxidative dehydrogenation of ethane and propane: how far from commercial implementation? *Catal. Today* 127 (2007) 113–131.
- [5] D. Melzer, P. Xu, D. Hartmann, Y. Zhu, N.D. Browning, M. Sanchez-Sanchez, J.A. Lercher, Atomic-scale determination of active facets on the MoVTeNb oxide M1 phase and their intrinsic catalytic activity for ethane oxidative dehydrogenation, *Angew. Chem. Int. Ed.* 55 (2016) 8873–8877.
- [6] B. Chu, H. An, X. Chen, Y. Cheng, Phase-pure M1  $MoVNbTeO_x$  catalysts with tunable particle size for oxidative dehydrogenation of ethane, *Appl. Catal. A: Gen.* 524 (2016) 56–65.
- [7] E. Heracleous, A.F. Lee, K. Wilson, A.A. Lemonidou, Investigation of Ni-based alumina-supported catalysts for the oxidative dehydrogenation of ethane to ethylene: structural characterization and reactivity studies, *J. Catal.* 231 (2005) 159–171.
- [8] Z. Skoufa, G. Xantri, E. Heracleous, A.A. Lemonidou, A study of  $Ni-Al-O$  mixed oxides as catalysts for the oxidative conversion of ethane to ethylene, *Appl. Catal. A: Gen.* 471 (2014) 107–117.
- [9] B. Savova, S. Lordinat, D. Filkova, J.M.M. Millet,  $Ni-Nb-O$  catalysts for ethane oxidative dehydrogenation, *Appl. Catal. A: Gen.* 390 (2010) 148–157.
- [10] J.M.L. Nieto, B. Solsona, R.K. Grasselli, P. Concepción, Promoted  $NiO$  catalysts for the oxidative dehydrogenation of ethane, *Top. Catal.* 57 (2014) 1248–1255.
- [11] H. Zhu, D.C. Rosenfeld, D.H. Anjum, V. Caps, J.-M. Basset, Green synthesis of  $Ni-Nb$  oxide catalysts for low-temperature oxidative dehydrogenation of ethane, *ChemSusChem* 8 (2015) 1254–1263.
- [12] P. Botella, A. Dejoz, M.C. Abello, M.I. Vázquez, L. Arrúa, J.M.L. Nieto, Selective oxidation of ethane: developing an orthorhombic phase in  $Mo-V-X$  ( $X = Nb, Sb, Te$ ) mixed oxides, *Catal. Today* 142 (2009) 272–277.
- [13] T.T. Nguyen, M. Aouine, J.M.M. Millet, Optimizing the efficiency of MoVTeNbO catalysts for ethane oxidative dehydrogenation to ethylene, *Catal. Commun.* 21 (2012) 22–26.
- [14] J.S. Valente, H. Armendáriz-Herrera, R. Quintana-Solórzano, P. del Ángel, N. Nava, A. Massó, J.M.L. Nieto, Chemical, structural, and morphological changes of a MoVTeNb catalyst during oxidative dehydrogenation of ethane, *ACS Catal.* 4 (2014) 1292–1301.
- [15] E.M. Thorsteinson, T.P. Wilson, F.G. Young, P.H. Kasai, The oxidative dehydrogenation of ethane over catalysts containing mixed oxides of molybdenum and vanadium, *J. Catal.* 52 (1978) 116–132.

[16] Y. Gao, L.M. Neal, F. Li, Li-promoted  $\text{La}_x\text{Sr}_{2-x}\text{FeO}_{4-8}$  core–shell redox catalysts for oxidative dehydrogenation of ethane under a cyclic redox scheme, *ACS Catal.* 6 (2016) 7293–7302.

[17] C.P. Kumar, S. Gaab, T.E. Müller, J.A. Lercher, Oxidative dehydrogenation of light alkanes on supported molten alkali metal chloride catalysts, *Top. Catal.* 50 (2008) 156–167.

[18] C.A. Gärtnner, A.C. van Veen, J.A. Lercher, Oxidative dehydrogenation of ethane on dynamically rearranging supported chloride catalysts, *J. Am. Chem. Soc.* 136 (2014) 12691–12701.

[19] S. Gaab, M. Machli, J. Find, R.K. Grasselli, J.A. Lercher, Oxidative dehydrogenation of ethane over novel Li/Dy/Mg mixed oxides: structure–activity study, *Top. Catal.* 23 (2003) 151–158.

[20] B.C. Michael, D.N. Nare, L.D. Schmidt, Catalytic partial oxidation of ethane to ethylene and syn gas over Rh and Pt coated monoliths: spatial profiles of temperature and composition, *Chem. Eng. Sci.* 65 (2010) 3893–3902.

[21] B. Fu, J. Lu, P.C. Stair, G. Xiao, M.C. Kung, H.H. Kung, Oxidative dehydrogenation of ethane over alumina-supported Pd catalysts. Effect of alumina overlayer, *J. Catal.* 297 (2013) 289–295.

[22] E.K. Novakova, J.C. Védrine, E.G. Derouane, Ammonoxidation of propane over catalysts comprising mixed oxides of Mo and V, *J. Catal.* 211 (2002) 235–243.

[23] T. Ushikubo, H. Nakamura, Y. Koyasu, S. Wajiki, Method for producing an unsaturated carboxylic acid, US patent 5,380,933, January 10 (1995).

[24] J.M.L. Nieto, P. Botella, M.I. Vázquez, A. Dejoz, The selective oxidative dehydrogenation of ethane over hydrothermally synthesised MoVTeNb catalysts, *Chem. Commun.* (2002) 1906–1907.

[25] B. Chu, L. Truter, T.A. Nijhuis, Y. Cheng, Performance of phase-pure M1 MoVNbTeOx catalysts by hydrothermal synthesis with different post-treatments for the oxidative dehydrogenation of ethane, *Appl. Catal. A: Gen.* 498 (2015) 99–106.

[26] B. Solsona, M.I. Vázquez, F. Ivars, A. Dejoz, P. Concepción, J. Nieto, Selective oxidation of propane and ethane on diluted Mo–V–Nb–Te mixed-oxide catalysts, *M. L. J. Catal.* 252 (2007) 271–280.

[27] B. Chu, H. An, T.A. Nijhuis, J.C. Schouten, Y. Cheng, A self-redox pure-phase M1 MoVNbTeOx/CeO<sub>2</sub> nanocomposite as a highly active catalyst for oxidative dehydrogenation of ethane, *J. Catal.* 329 (2015) 471–478.

[28] E.V. Ishchenko, R.V. Gulyaev, T.Y. Kardasha, A.V. Ishchenko, E.Y. Gerasimov, V.I. Sobolev, V.M. Bondareva, Effect of Bi on catalytic performance and stability of MoVTeNbO catalysts in oxidative dehydrogenation of ethane, *Appl. Catal. A: Gen.* 534 (2017) 58–69.

[29] E.V. Ishchenko, T.Y. Kardasha, R.V. Gulyaev, A.V. Ishchenko, V.I. Sobolev, V.M. Bondarev, Effect of K and Bi doping on the M1 phase in MoVTeNbO catalysts for ethane oxidative conversion to ethylene, *Appl. Catal. A: Gen.* 514 (2016) 1–13.

[30] T. Montini, M. Melchionna, M. Monai, P. Fornasiero, Fundamentals and catalytic applications of CeO<sub>2</sub>-based materials, *Chem. Rev.* 116 (2016) 5987–6041.

[31] H. Watanabe, Y. Koyasu, New synthesis route for Mo–V–Nb–Te mixed oxides catalyst for propane ammonoxidation, *Appl. Catal. A: Gen.* 194–195 (2000) 479–485.

[32] G. Kresse, J. Furthmüller, Efficient iterative schemes for ab initio total-energy calculations using a plane-wave basis set, *Phys. Rev. B* 54 (1996) 11169–11186.

[33] J.P. Perdew, K. Burke, M. Ernzerhof, Generalized gradient approximation made simple, *Phys. Rev. Lett.* 77 (1996) 3865–3868.

[34] P.E. Blöchl, Projector augmented-wave method, *Phys. Rev. B* 50 (1994) 17953–17979.

[35] C. Sun, H. Li, L. Chen, Nanostructured ceria-based materials: synthesis, properties, and applications, *Energy Environ. Sci.* 5 (2012) 8475–8505.

[36] X. Yao, C. Tang, Z. Ji, Y. Dai, Y. Cao, F. Gao, L. Dong, Y. Chen, Investigation of the physicochemical properties and catalytic activities of Ce<sub>0.67</sub>M<sub>0.33</sub>O<sub>2</sub> (M = Zr<sup>4+</sup>, Ti<sup>4+</sup>, Sn<sup>4+</sup>) solid solutions for NO removal by CO, *Catal. Sci. Technol.* 3 (2013) 688–698.

[37] J.M. Oliver, J.M.L. Nieto, P. Botella, A. Mifsud, The effect of pH on structural and catalytic properties of MoVTeNbO catalysts, *Appl. Catal. A: Gen.* 257 (2004) 67–76.

[38] X.-J. Yang, R.-M. Feng, W.-J. Ji, C.-T. Au, Characterization and evaluation of Mo–V–Te–Nb mixed metal oxide catalysts fabricated via hydrothermal process with ultrasonic pretreatment for propane partial oxidation, *J. Catal.* 253 (2008) 57–65.

[39] X. He, X. Liu, R. Li, B. Yang, K. Yu, M. Zeng, R. Yu, Effects of local structure of Ce<sup>3+</sup> ions on luminescent properties of Y<sub>3</sub>Al<sub>5</sub>O<sub>12</sub>–Ce nanoparticles, *Sci. Rep.* 6 (2016) 22238.

[40] E. Béche, P. Charvin, D. Perarnau, S. Abanades, G. Flamant, Ce 3d XPS investigation of cerium oxides and mixed cerium oxide (Ce<sub>x</sub>Ti<sub>y</sub>O<sub>2</sub>), *Surf. Interface Anal.* 40 (2008) 264–267.

[41] H. Zhu, P. Laveille, D.C. Rosenfeld, M.N. Hedhilić, J.-M. Basset, A high-throughput reactor system for optimization of Mo–V–Nb mixed oxide catalyst composition in ethane ODH, *Catal. Sci. Technol.* 5 (2015) 4164–4173.

[42] V.D.B.C. Darierddy, M. Huš, B. Likozar, Effect of O<sub>2</sub>, CO<sub>2</sub> and N<sub>2</sub>O on Ni–Mo/Al<sub>2</sub>O<sub>3</sub> catalyst oxygen mobility in n-butane activation and conversion to 1,3-butadiene, *Catal. Sci. Technol.* 7 (2017) 3291–3302.

[43] E.K. Novakova, J.C. Védrine, E.G. Derouane, Propane oxidation on Mo–V–Sb–Nb mixed oxide catalysts: 2. Influence of catalyst activation methods on the reaction mechanism, *J. Catal.* 211 (2002) 235–243.